Ultrasonics Sonochemistry 100 (2023) 106644

Contents lists available at ScienceDirect

Ultrasonics Sonochemistry

journal homepage: www.elsevier.com/locate/ultson

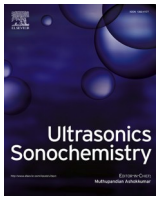

Increased intracellular diffusivity of macromolecules within a mammalian cell by low-intensity pulsed ultrasound

Hyojun Kim [a], Yeonho Choi [b], So Yeon Kim [c,d,*], Ki Joo Pahk [e,*]

[a] LAAS-CNRS, University of Toulouse, CNRS, Toulouse, France
[b] Department of Bioengineering, Korea University, Seoul, Republic of Korea
[c] Chemical and Biological Integrative Research Center, Biomedical Research Division, Korea Institute of Science and Technology (KIST), Seoul, Republic of Korea
[d] Division of Bio-Medical Science and Technology, KIST School, Korea University of Science and Technology (UST), Seoul 02792, Republic of Korea
[e] Department of Biomedical Engineering, Kyung Hee University, Yongin 17104, Republic of Korea

ARTICLE INFO

Keywords:
Low intensity pulsed ultrasound
Intracellular dynamics
Cytoplasmic diffusion
Molecular diffusivity
Nucleocytoplasmic transport
Kinase activity

ABSTRACT

Whilst a number of studies have demonstrated that low-intensity pulsed ultrasound (LIPUS) is a promising therapeutic ultrasound technique that can be used for delivering mild mechanical stimuli to target tissue non-invasively, the underlying biophysical mechanisms still remain unclear. Most mechanism studies have focused explicitly on the effects of LIPUS on the cell membrane and mechanosensitive receptors. In the present study, we propose an additional mechanism by which LIPUS propagation through living cells may directly impact intracellular dynamics, particularly the diffusion transport of biomolecules. To support our hypothesis, human epithelial-like cells (SaOS-2 and HeLa) seeded on a confocal dish placed on a microscope stage were exposed to LIPUS with various exposure conditions (ultrasound frequencies of 0.5, 1 and 3 MHz, peak acoustic pressure of 200 and 400 kPa, a pulse repetition frequency of 1 kHz and a 20 % duty cycle), and the diffusivities of various sizes of biomolecules in the cytoplasm area were measured using fluorescence recovery after photobleaching (FRAP). Furthermore, giant unilamellar vesicles (GUVs) filled with macromolecules were used to examine the physical causal relationship between LIPUS and molecular diffusion changes. Nucleocytoplasmic transport coefficients were also measured by modified FRAP that bleaches the whole cell nuclear region. Extracellular signal-regulated kinases (ERK) activity (the phosphorylation dynamics) was monitored using fluorescence resonance energy transfer (FRET) microscopy. All the measurements were taken during, before and after the LIPUS exposure. Our experimental results clearly showed that the diffusion coefficients of macromolecules within the cell increased with acoustic pressure by 12.1 to 33.5 % during the sonication, and the increments were proportional to their molecular sizes regardless of the ultrasound frequency used. This observation in living cells was consistent with the GUVs exposed to the LIPUS, which indicated that the diffusivity increase was a passive physical response to the acoustic energy of LIPUS. Under the 1 MHz LIPUS exposure with 400 kPa, the passive nucleocytoplasmic transport of enhanced green fluorescent protein (EGFP) was accelerated by 21.4 %. With the same LIPUS exposure condition, both the diffusivity and phosphorylation of ERK induced by EGF treatment were significantly elevated simultaneously, which implied that LIPUS could also modify the kinase kinetics in the signal transduction process. Taken together, this study is the first attempt to uncover the physical link between LIPUS and the dynamics of intracellular macromolecules and related biological processes that LIPUS can possibly increase the diffusivity of intracellular macromolecules, leading to the changes in the basic cellular processes: passive nucleocytoplasmic transport and ERK. Our findings can provide a novel perspective that the mechanotransduction process that the intracellular region, in addition to the cell membrane, can convert the acoustic stimuli of LIPUS to biochemical signals.

* Corresponding authors at: Department of Biomedical Engineering, Kyung Hee University, Yongin, Republic of Korea (K. J. Pahk); Chemical and Biological Integrative Research Center, Biomedical Research Division, Korea Institute of Science and Technology (KIST), Seoul, Republic of Korea (S. Y. Kim).
E-mail addresses: soyeonkim@kist.re.kr (S.Y. Kim), kjpahk@khu.ac.kr (K.J. Pahk).

https://doi.org/10.1016/j.ultsonch.2023.106644
Received 21 July 2023; Received in revised form 5 October 2023; Accepted 7 October 2023
Available online 10 October 2023

1. Introduction

Low-intensity pulsed ultrasound (LIPUS) is a specific type of therapeutic ultrasound technique that delivers low acoustic energy into target tissue noninvasively for cell stimulation [1]. The pulsed wave mode used in LIPUS prevents the bulk temperature rising and mechanical disruption of the target tissue while maintaining a moderate level of mechanical stimulation [2]. The biological effects of LIPUS have been well demonstrated in a number of studies for clinical applications, including bone-fracture healing [3,4], soft-tissue regeneration [5–7], inflammatory response inhibition [8,9] and neuromodulation [10,11]. Despite the promising beneficial effects of LIPUS reported, the underlying physical and molecular mechanisms of how LIPUS interacts with cells or tissues remain obscure [12,13]. A number of potential mechanisms have been proposed.

Most biophysical mechanisms studies on LIPUS treatment have mainly paid attention to the cell membrane in which acoustic stimulation has transformed into biological signals [14]. Ultrasound with low intensity can deform the lipid membrane tension by acoustic radiation force [15] or by a direct mechanical interaction between the membrane and acoustic wave [16,17], stimulating mechanosensitive receptors and channels to trigger the signaling cascades. In contrast to the cell membrane, the interaction of LIPUS with the intracellular domain has barely been considered a potential mechanism. The cell interior is a complex aqueous environment crowded with a large number of subcellular organelles, biopolymers and other molecules [18,19]. External forces can directly impact the intracellular domain modifying subcellular organelle physiology [20,21] and molecular crowding [22]. It has been reported that the reaction rate of many biochemical reactions depends on the diffusion process (i.e., diffusion-limited process) [23] and the diffusion of biological macromolecules can be slowed down by its crowded environment. The time taken for proteins within a cell to encounter their targets during cellular processes such as signaling cascade [24], nucleocytoplasmic transport [25] and cytoskeletal dynamic [26,27] depends partly on how fast the proteins can diffuse. Along with these, the intracellular diffusion can also be affected by changes in pH level [28], osmotic pressure [29] and growth-induced pressure [22]. With these contexts and given the nature of how ultrasound travels through a medium, we hypothesise that, in addition to the cell membrane, LIPUS can possibly alter the intracellular environment triggering the signaling cascades (e.g., pressure oscillation of intracellular biomolecules within the ultrasound beam path) whilst propagating through a cell or cell cluster. Physical and biological responses of the cell interior to LIPUS exposure are, however, largely unknown.

To that end, the main objective of the present study is, therefore, to provide better insights into the mechanisms of LIPUS stimulation by investigating the potential effect of LIPUS on the intracellular environment, particularly the molecular diffusivity within the cell interior. In the present study, an *in vitro* experiment with an epithelial human cell line, SaOS-2 or HeLa cells, embedded in a confocal dish under various LIPUS exposure conditions was carried out. The diffusivity of macromolecules with various sizes (4 to 500 kDa) injected or genetically expressed in the cytoplasm region was measured using fluorescence recovery after photobleaching (FRAP). A cell-mimicking model with giant unilamellar vesicles (GUVs) was employed to verify the diffusivity changes due to LIPUS at a cell. Then, the passive nucleocytoplasmic rate of enhanced green fluorescent protein (EGFP) was quantified under LIPUS exposure by modified FRAP that bleaches the whole cell nuclear region. Lastly, extracellular signal-regulated kinases (ERK) phosphorylation dynamics during both epidermal growth factor (EGF) and LIPUS stimulations were monitored by fluorescence resonance energy transfer (FRET) microscopy.

2. Materials and Methods

2.1. LIPUS experimental setup and acoustic pressure field calibration

The ultrasound stimulator used in the present study was designed to be used in conjunction with a confocal microscope for simultaneous microscopic observation of the changes of biomolecules in cells during LIPUS exposure, as shown in Fig. 1a. The LIPUS stimulator filled with degassed water was placed on the top of a confocal dish, which has a 180 μm thick polymer coverslip bottom for adherent cell culture (80136, ibidi, Germany), to stimulate adherent cells while monitoring changes in cells in real-time with an inverted microscope. An unfocused ultrasound planar transducer operating at 0.5, 1 or 3 MHz with a 10 mm diameter (DONG IL Technology Ltd, Republic of Korea) was integrated to the stimulator. The ultrasound was delivered to the cells at an incident angle of 40° to minimise potential standing wave formation. An acoustic absorber was also put on the opposite side of the transducer to prevent undesired acoustic reflections. The distance between the surface of the transducer and the target cells on the confocal dish was 30 mm. An acoustically transparent polyethylene (i.e., Mylar) film was placed at the bottom of the stimulator for coupling purpose. A function generator (33500B, Keysight, US) and a power amplifier (210L, Electronics & Innovation, US) were used to drive the transducer. Various LIPUS exposure conditions with a pulse repetition frequency (PRF) of 1 kHz, pulse duration of 200 μs, peak acoustic pressure of 200 and 400 kPa and 20 % duty cycle were employed in the present study. These conditions have been widely used in many clinical applications [1]. The 2D spatial distribution of acoustic pressure fields along the cell culture area of a confocal dish was experimentally measured (Fig. 1c). Under a given LIPUS exposure condition, the acoustic pressure amplitude at the center surface of the cell dish along the transducer's axial axis was measured using a calibrated hydrophone (HNR-500, ONDA, US) and a digital oscilloscope (DPO 4104, Tektronix, US) with a sampling frequency of 0.1 GHz, as shown in Fig. 1c. The position of the hydrophone was controlled by a three-axis positioning system (Bi-Slide Velmex, Inc. Bloomfield, US). All data in this study were acquired from the cells placed within the circular area with the diameter of the full width at half maximum (FWHM) of the acoustic pressure (Fig. 1d). All the LIPUS stimulation protocols used in the present study did not adversely affect the cytoskeletal structure and cell viability, and the bulk temperature increase during the LIPUS treatment was measured to be less than 1 K.

2.2. Cell culture and reagents

SaOS-2 cells and HeLa cells, obtained from Korean Cell Line Bank (Republic of Korea), were cultured in Dulbecco's Modified Eagle Medium (DMEM; 11995065, Gibco, US) supplemented with 10 % v/v heat-inactivated fetal bovine serum (hiFBS; 10082147, Gibco, US), 100 μg/mL penicillin and 100 μg/mL streptomycin, and the cells were maintained under 5 % CO_2 at 37 °C in a humidified incubator. Prior to the experiments, 3×10^5 cells were seeded onto confocal dishes with 35 and 50 mm diameters (80136, ibidi, Germany) for the FRAP and FRET experiments, respectively. The cell culture medium was changed into phenol-red free DMEM (21063–029, Gibco, US) with 25 mM HEPES (H0887, Sigma-Aldrich, US) at least 8 hours before the measurements. Cells were treated with Gadolinium (439880, Sigma-Aldrich, US) at 20 μM concentration 10 min prior to the measurements [30].

2.3. Transfections

All transfections were conducted using Lipofectamine™ 3000 (L3000008, Invitrogen, Thermo Fisher Scientific, US), following the recommended protocol by manufacturer. pcDNA3-EGFP was a gift from Doug Golenbock (Addgene plasmid # 13031; https://n2t.net/addgene:13031; RRID:Addgene_13031). GFP-ERK1 was a gift from Rony Seger (Addgene plasmid # 14,747; https://n2t.net/addgene:14747;

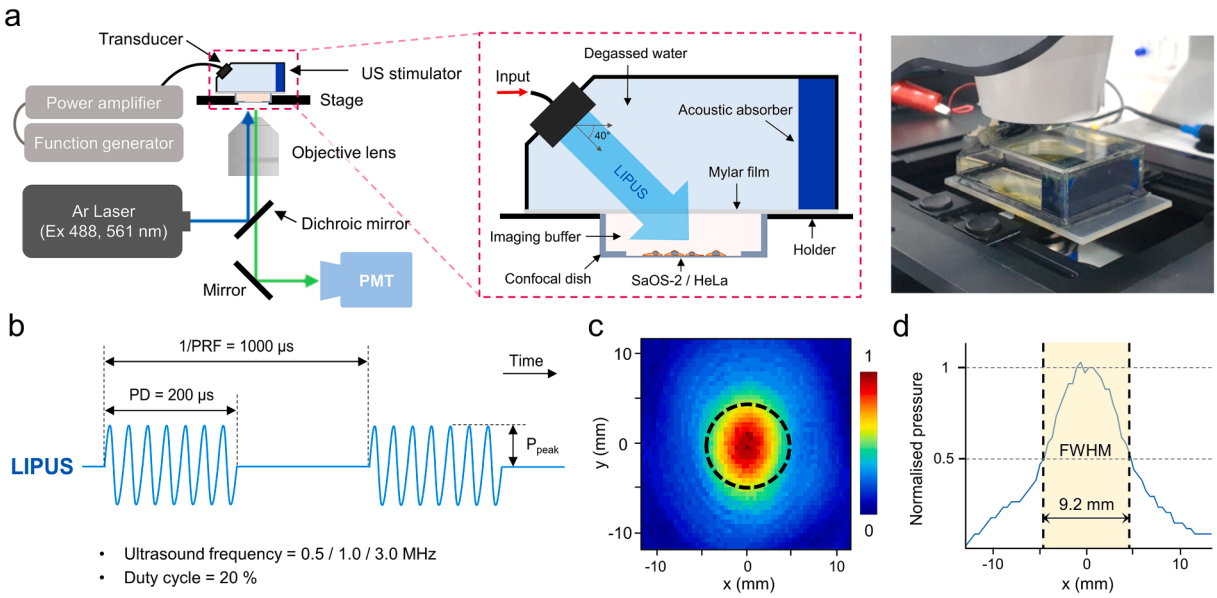

Fig. 1. (a) Illustration and image of the LIPUS stimulation and imaging setup. Live-cell imaging and FRAP measurements were conducted during LIPUS exposure on an inverted confocal microscope. (b) Schematic of the acoustic waveform of LIPUS applied to SaOS-2 and HeLa cells. (c) The normalised lateral 2D beam profile of LIPUS used in this study was measured in degassed water along the plane on which the samples (i.e., cells or GUVs) were to be placed. A colour bar represents normalised acoustic pressure, and the dashed black circle indicates the full width at half maximum (FWHM) pressure contour along the lateral coordinate (x-axis). (d) The normalised 1D beam profiles were demonstrated and the 9.2 mm of FWHM acoustic pressure along the x-axis was extracted by Gaussian fitting.

RRID:Addgene_14747) [31]. cytoplasmic EKAR(EGFP-mRFP) plasmid was a gift from Karel Svoboda (Addgene plasmid # 18,680; https://n2t.net/addgene:18680; RRID:Addgene_18680) [32]. mCherry-DN KASH/EA plasmid was a gift from Daniel Conway (Addgene plasmid #125553; https://n2t.net/addgene:125553; RRID:Addgene_125553) [33].

2.4. Glass beads loading

Glass bead loading is a rapid and simple technique for loading large numbers of cultured cells with large macromolecules [34]. FITC-dextrans (FD-S series, Sigma-Aldrich, US) with various molecular weights (4, 70 and 500 kDa) were dissolved at a concentration of 10 mg/mL in Dulbecco's phosphate buffered saline (DPBS). After two-time rinse of the cells cultured on a confocal dish using DPBS, 1 mL of FITC-dextran solution was pipetted onto the cells. 200 mg of Acid-washed glass beads of 425–600 μm diameter (G8772, Sigma-Aldrich, US) were then carefully and evenly sprinkled onto the cell culture area of the confocal dish. Beads were allowed to roll around on top of the cells until evenly distributed over their surface and afterward, the cells were rinsed by dipping the whole confocal dish in a DPBS bath (>50 mL). Then, the cells were incubated with the culture medium and allowed to recover in a cell incubator. Cells were further incubated at least 8 hours before the FRAP experiments.

2.5. Osmotic stress

Hyperosmotic stress (400 mOsm/kg) was applied by changing the cell culture medium to the hyperosmotic medium, which is DMEM supplemented with 3.0 wt% polyethylene glycol 400 (PEG / 202398, Sigma-Aldrich, US), and the cells were incubated 5 min before imaging. The weight concentration value of PEG 400 solution was obtained from the previous report [35].

2.6. Confocal fluorescence imaging

The cells were imaged by a confocal laser-scanning microscope (LSM 800, Carl Zeiss, Germany) with a 20×/NA 0.8 DIC PlanApo dry objective and 63×/NA 1.4 DIC PlanApo oil-immersion objective, depending on the measurements. For EGFP and FITC, a diode laser (488 nm) was used for excitation, and the emission was collected from 530 to 630 using the spectral detection system. RFP and mCherry were excited at 561 nm using a diode laser, and the emission was collected from 590 to 620 nm.

2.7. FRAP and diffusion coefficient measurement

FRAP experiments were performed on the same confocal microscope stated above using a 63×/NA 1.4 DIC PlanApo oil-immersion objective. The imaging window was selected as a horizontal strip shape (10 × 3 μm or 5 × 3 μm, depending on the experimental sample, 1 px = 0.1 μm) to minimise the image acquisition time (scan speed 0.53 μsec/px, 18.58 or 13.68 ms frame time). Samples were imaged and bleached using a 30 mW Argon laser (488 nm) and the laser power for fluorescence images was maintained between 6.5 and 10 nW (488 nm). Each FRAP experiment was conducted only one time per sample (i.e., a cell or a GUV) per condition at room temperature (23 °C). The bleaching of EGFP and FITC was achieved by focusing the 488 nm laser light with maximum power on a circular region (r = 1.5 μm). In the case of cells, the bleaching position was arbitrarily selected within the cytoplasmic area so that the bleaching area did not contain part of the cell nucleus or cell exterior. All FRAP experiments under LIPUS exposure were carried out within the first 3 min of the sonication. Furthermore, to correct any diffusion that occurs during photobleaching and the time taken to acquire the first image, the effective radius r_e was extracted from the Gaussian fit of postbleaching profile [36] (Supplementary Fig. 1a). The postbleaching profile was obtained from the first captured fluorescence image after the bleaching, radially integrated over a full angle ($\theta = 360°$) to obtain 1D profiles of intensity against the distance (r) from the center of the bleached area. The profile was normalised by the mean prebleach fluorescence intensity (N = 10). Then, the normalised profile was fitted to [36]

$$C_{\text{postbleach}}(r) = 1 - K\exp\left(-\frac{r^2}{r_e^2}\right) \quad (1)$$

where K is the bleaching depth minimising the sum of mean-square errors by use of OriginPro 9.0 (OriginLab Corporation, US). Diffusivity of

macromolecules was calculated by fitting the recovery curve [37,38] (Supplementary Fig. 2b). A solution of the implicit equation with unknown diffusion coefficient D and an initial condition given by equation (2), a numerical equation for FRAP can be presented as [36]

$$F(t) = F_i\left\{1 - \frac{K}{1+\gamma^2+2t/\tau_D}\right\}M_i + (1-M_f)F_0 \quad (2)$$

where $\tau_D = r_e^2/(4D)$ and $\gamma = r_n/r_e.M_f$ is defined as

$$M_f = \frac{F_\infty - F_0}{F_i - F_0} \quad (3)$$

where F_i is prebleach fluorescence intensity average with 10 images, F_0 is the postbleach initial fluorescence intensity and F_∞ is the postbleach steady-state fluorescence intensity.

2.8. GUV formation and vesicle immobilization

GUVs were electroformed on stainless steel electrodes [39]. In brief, solutions of 1,2-distearoyl-*sn*-glycero-3-phosphocholine (DOPC) (25 mg/mL in chloroform) and cholesterol (10 mg/mL in chloroform) were mixed at 1:1 molar fractions. 1,2-dipalmitoyl-*sn*-glycero-3 phosphoethanolamine-N-(cap-biotinyl) sodium salt (DPPE-biotin) was then added to the solution at 1 mol% for vesicle immobilisation on the glass surface of confocal dish. The resulting solution was then pipetted vertically onto a pair of stainless-steel electrodes (50 µl per pair). After drying, the electroformation chamber was filled within sucrose solution (~3 mL, 200 mM sucrose in MilliQ deionised water at 23 °C) in which 10 mg/mL of FITC-dextran was solved, the electrodes were submerged, and the function generator was connected using brass rods on the chamber sides. A 10 Hz, 5 V peak-to-peak voltage (V_{pp}) sinusoidal excitation was then applied for 2 h, followed by 30 min at a lower frequency of 5 Hz to facilitate vesicle detachment. The vesicle with a range between 30 and 50 µm in diameter were manually selected for FRAP experiments.

The vesicles were immobilised on a confocal dish using avidin–biotin chemistry. First, the imaging region (glass coverslip) of confocal dish was coated with 400 µl of biotin labelled bovine serum albumin (bBSA) solution (10 mg/mL in PBS) for two hours at room temperature. After washing with deionised water, an avidin solution (1 mg/mL in PBS) was pipetted on the plate and incubated for four hours. After repeated washing with PBS, a 500 µl of biotin labelled GUV solution was added and allowed to attach on the surface for 30 min. The lipid shell structure of GUV was labelled with a 1.0 µg/ml concentration of Nile red (72485, Sigma-Aldrich, US) solution. The vesicles with 30–50 µm of diameter for FRAP experiment were measured and selected manually using LSM 800 confocal microscope.

2.9. Nucleus-cytoplasmic translocation rate measurement using FRAP

The cells were imaged with a 20×/NA 0.8 DIC PlanApo objective, and the focus was adjusted in the middle plane of the nucleus. For FRAP analysis, the whole nucleus area was manually selected and photobleached for 3 sec with maximum laser power (488 nm) until a less than 80 % reduction of initial fluorescence intensity. The fluorescence images were obtained every 2 sec for 10 min. In all cases, the time-dependent intensity rise calculated by taking the averaged (background-corrected) nucleus fluorescence intensity, $F(t)$ was fitted to a single-exponential curve with an equation as follows [40,41],

$$F(t) = F_{max}(1 - e^{-kt}) \quad (4)$$

where t is the time, and k is the first order rate constant, nucleocytoplasmic transport rate. All transport rates used in the present study were extracted from qualified curves with the R^2 value (>0.95).

2.10. Ratiometric FRET measurement

Cytoplasmic EKAR (EGFP-mRFP), a FRET-based sensor of ERK activity (the extracellular signal-regulated kinase activity reporter), was used for the analysis of ERK signaling in living cells [32,41]. Cells were starved for at least 12 hours to inhibit ERK activity and then stimulated with EGF. Cells were imaged in phenol red-free DMEM medium using LSM 800 laser-scanning confocal microscope using a heated stage and CO2 supply with a 40×/1.20NA Plan Apo objective. For ratiometric FRET analysis, EGFP images were captured with an EGFP excitation and EGFP emission filter, and mRFP images were defined as fluorescence images with an EGFP excitation and mRFP emission filter. Then, mRFP images were divided by EGFP images to obtain mRFP/GFP ratio, which is defined as FRET efficiency. The acquisition time interval was 30 sec, and the whole observation time span was 20 min. 5 min after the acquisition started, 100 µl of concentrated EGF solution was injected carefully to reach the concentration of 50 ng/mL [42,43], then the cell media was homogenised by multiple pipetting towards the inner wall of the dish. The data analysis for FRET efficiency for each data analysis was conducted with the ImageJ software described in the other protocol [44]. The ratio of acceptor and donor fluorescent intensities was calculated with flat field images for each channel after the background correction process. Normalised curves were obtained by dividing the average of the pre-stimulated images (time points −5 to 0 min) for each time point.

2.11. Data and statistical analysis

All image analysis was performed using ImageJ (National Institutes of Health, US) and its plug-in package, Fiji. Statistical analysis was performed with GraphPad Prism 9.0.0 (Dotmatics, US) with one-way ANOVA for multiple comparison analysis, while a Student's *t*-test was used for direct comparison between two data sets. All data are expressed in terms of mean ± standard deviation (SD) and the number of independent replicates is expressed in the figure captions. Following conventions for statistical significance are used throughout the experiments: ns = $p > 0.05$, * = $p \leq 0.05$, ** = $p \leq 0.01$, *** = $p \leq 0.001$, **** = $p \leq 0.0001$.

3. Results

3.1. LIPUS stimulation increases the diffusivity of cytoplasmic macromolecules

To explore the effect of LIPUS stimulation on the diffusion behaviour of biomolecules in a human cell, we initially introduced various biologically inert fluorescent probe molecules with a wide range of molecular weights into the cytoplasm of SaOS-2 and HeLa cells. As a probe molecule, EGFP (27 kDa) was expressed in a cell by transient transfection, or fluorescein isothiocyanate (FITC) conjugated-dextran with different molecular weights (4, 70 and 500 kDa) was injected in the cytoplasm using the glass bead loading method (see Materials and Methods 2.4). The diffusion coefficient of each probe molecule was measured using FRAP (see Materials and Methods 2.7) analysis. The FRAP measurements under LIPUS exposure were conducted within 3 min of sonication to minimise the interference with cellular responses to external stresses. In the absence of the LIPUS exposure, the diffusion coefficient of 70 kDa FITC-Dextran in the SaOS-2 cytoplasm (D) was initially determined as 15.9 ± 3.5 µm^2/s (mean ± standard deviation) (Fig. 2b). This was comparable to the value reported in previous studies [45,46]. Interestingly, in our experiments, we observed that the diffusion coefficient of 70 kDa FITC-Dextran increased during the 1 MHz LIPUS exposure (17.0 ± 3.2 µm^2/s with 200 kPa) which was then further increased with increasing the acoustic pressure (18.8 ± 3.1 µm^2/s with

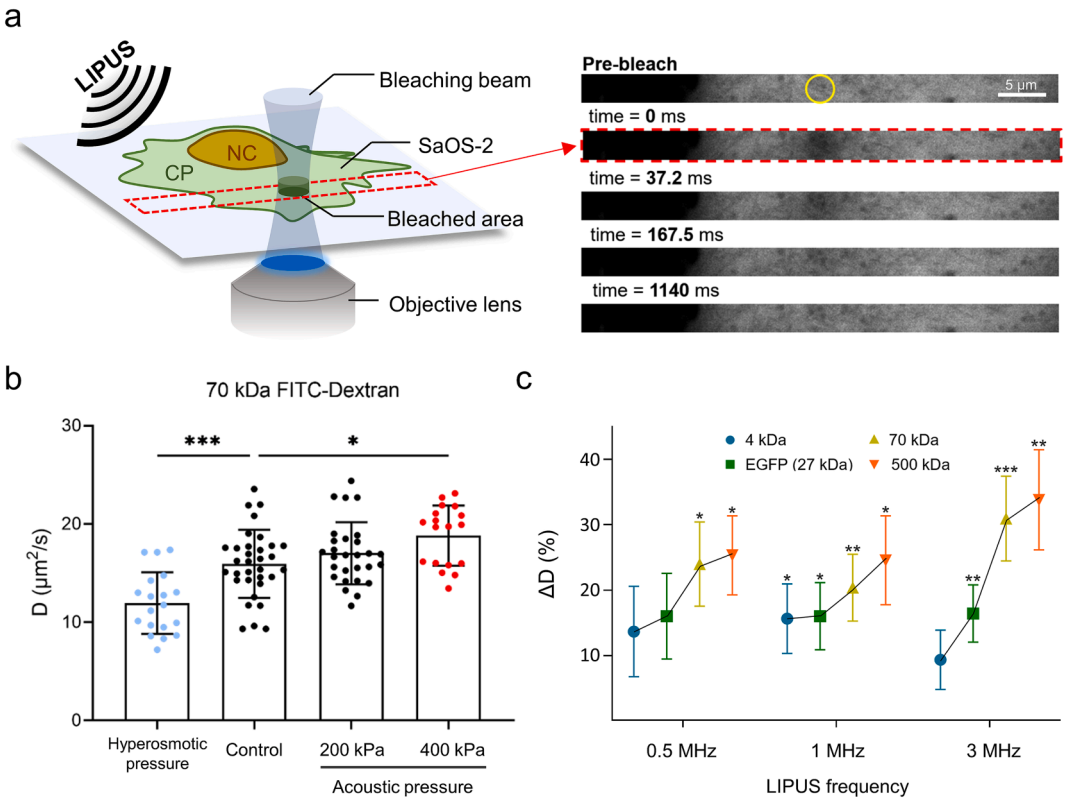

Fig. 2. (a) Illustration of FRAP experiment during LIPUS stimulation on a SaOS-2 cell. The yellow circle in the prebleach image indicates the bleaching area ($r_n = 1.5$ μm) within the cytoplasm of SaOS-2 cells. After bleaching was executed, each image was acquired in 13.8 or 18.3 ms of time intervals. (b) Molecular diffusivity of 70 kDa FITC-dextran within the cytoplasm of SaOS-2 cell in the absence or presence of LIPUS stimulation (1 MHz) and hyperosmotic pressure (400 mOsm/kg). The statistically significant data is presented with different colours. (c) Percentage change of diffusivity of various samples with different molecular weights (GFP, 4 kDa, 70 kDa and 500 kDa of FITC-dextran) at 400 kPa acoustic pressure. Three different LIPUS frequencies (0.5, 1 and 3 MHz) were utilised. Values are expressed as mean ± SD of > 18 samples. * $P < 0.05$, ** $P < 0.01$ and *** $P < 0.001$. (For interpretation of the references to colour in this figure legend, the reader is referred to the web version of this article.)

400 kPa), whereas the diffusion coefficient under polyethylene glycol-induced hyperosmotic stress (400 mOsm/kg) decreased to 12.0 ± 0.7 $\mu m^2/s$ (Fig. 2b) which was comparable to the value reported in a previous study [47].

The effects of the variations of the molecular weight of the probe molecules (4, 27, 70 and 500 kDa) and ultrasound frequency (0.5, 1 and 3 MHz) on the diffusion coefficient at a constant acoustic pressure of 400 kPa were then examined. In all cases, the diffusion coefficient gradually increased with the molecular weight at a given LIPUS frequency (Fig. 2c and Supplementary Fig. 2a). These similar trends were also observed with HeLa cells (Supplementary Fig. 2b). From these experimental results, we therefore can conclude that LIPUS stimulation can increase the diffusivity of molecules in the cells. The heavier the molecules, the faster the diffusion rate under a given LIPUS exposure.

It has been reported that ultrasound stimulation can impact the cytoplasm's water or ion content by opening the mechanosensitive membrane channels, including Piezo1 [48] and TRP channels [17], possibly resulting in changes in cytoplasmic diffusion properties. To show that the changes in the diffusion coefficient of the probe molecules by the LIPUS stimulation observed in the present study did not result from the mechanosensitive ion channel opening, we treated the SaOS-2 cells with Gadolinium ion (Ga^{3+}) [30], which is a nonspecific blocker of mechanosensitive ion channels, prior to the LIPUS exposure. Interestingly, the molecular diffusivity again increased by the LIPUS stimulation (1 MHz, 200 and 400 kPa) with no significant differences between those with and without the Ga^{3+} ion pretreatment (Supplementary Fig. 2c). This shows that the increased molecular diffusivity by the LIPUS stimulation was not due to altered intracellular ionic distribution.

3.2. *The effect of LIPUS stimulation is consistently observed in a cell-mimicking model system with giant unilamellar vesicles (GUVs)*

To further demonstrate that the increase of diffusivity by LIPUS stimulation is a direct effect caused by the interaction between ultrasound waves and macromolecules, we used GUVs as a simplified cell-mimicking model [49,50] and measured the diffusion coefficient of FITC-Dextran (20, 70 and 500 kDa) in the GUV (Fig. 3a). The size of the prepared GUVs filled with FITC-dextran solution was in the range of 30 to 50 μm which was comparable to that of mammalian cells. GUVs were then attached to the glass surface of a confocal dish using biotin-avidin chemistry (Fig. 3b, see Materials and Methods 2.8).

Prior to LIPUS exposure, the diffusion coefficient of 70 kDa FITC-Dextran in the GUV was determined as 53.9 ± 9.9 $\mu m^2/s$ (mean ± standard deviation) (Fig. 3c), which was 3.39-fold greater than that of the SaOS-2 cell. This slower molecular diffusion rate inside the cytoplasm is likely to be due to the impeded mobility of molecules by a crowded environment of living cells [47,51]. As soon as the GUV vesicles were exposed to the 1 MHz LIPUS with 200 and 400 kPa, the diffusion coefficients of macromolecules in the GUV increased with the acoustic pressure amplitude (Fig. 3c). Similar to the results obtained with SaOS-2 cells depicted in Fig. 2c, the percentage increase in the diffusivity in the GUV was proportional to the size of the molecules (Fig. 3d). These results can imply that the increased macromolecular diffusivities within both the cytoplasm and GUV lumen under LIPUS exposure share the same principle, which is directly derived from the acoustic energy of LIPUS on the dynamics of macromolecules rather than via a biological reaction.

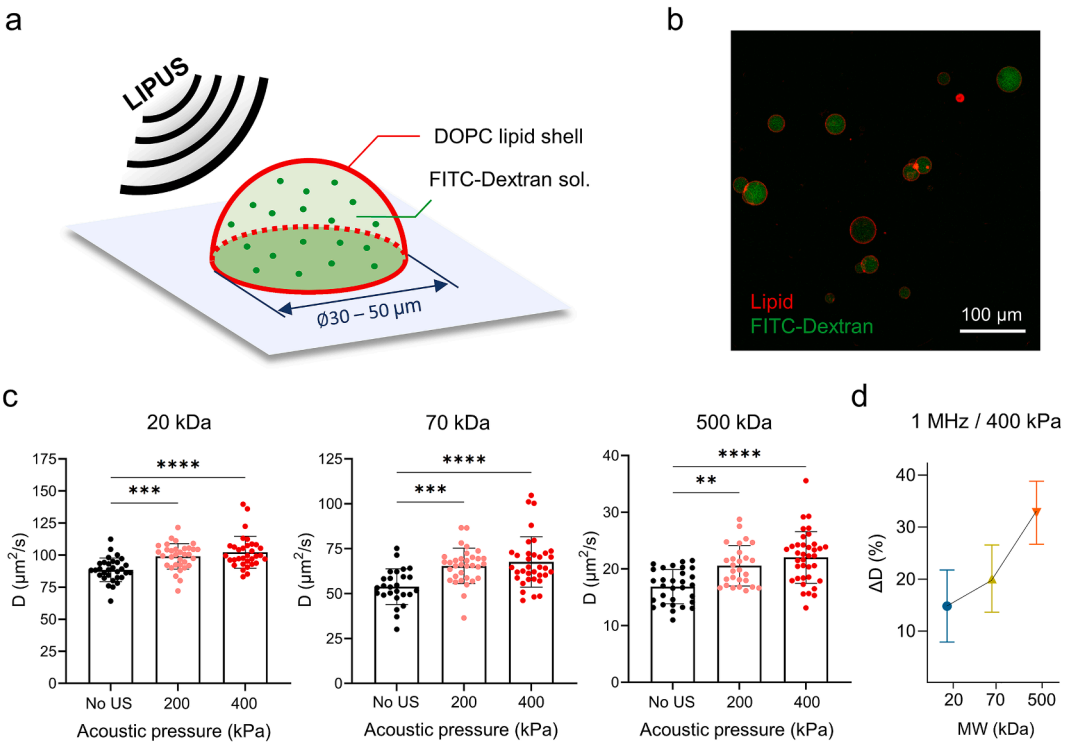

Fig. 3. (a) Illustration of LIPUS stimulation on a GUV containing FITC-dextran solution. (b) Representative fluorescence image of GUVs. FITC–dextran molecules filled in the GUV lumen and lipid membrane stained by Nile red are shown as green and red, respectively. (c) The effect of LIPUS stimulation (1 MHz) on the molecular diffusivity of FITC-dextrans. Three different FITC-dextrans with the molecular weight of 20, 70 and 500 kDa were utilised. The statistically significant data is presented with different colours. (d) Percentage change of diffusivity at 400 kPa acoustic pressure. Values are expressed as mean ± SD of > 20 samples. * $P < 0.05$, ** $P < 0.01$, *** $P < 0.001$, **** $P < 0.0001$. (For interpretation of the references to colour in this figure legend, the reader is referred to the web version of this article.)

3.3. *LIPUS stimulation accelerates passive nucleocytoplasmic transport rate*

On the basis of the experimental observations on the changes of the diffusivity of cytoplasmic macromolecules (Fig. 2), we hypothesised that LIPUS stimulation could also affect the kinetics of intracellular processes. To explore this possibility, we first considered nucleocytoplasmic transport. Nucleocytoplasmic transport of macromolecules through the nuclear membrane is a fundamental process for the signal transduction of eukaryotic cells [52]. In particular, small molecules such as ions, metabolites and intermediate-sized macromolecules can pass through the membrane by passive diffusion; however, this passive transport becomes increasingly restricted as the particle size approaches 60 to 70 kDa [25,53]. To investigate the potential effect of LIPUS stimulation on the passive nucleocytoplasmic transport, we measured the nucleocytoplasmic transport rate EGFP (27 kDa) expressed in SaOS-2 cells by FRAP analysis [40]. In the FRAP experiment, the nucleus area to be bleached was manually selected, and the recovery of fluorescent level of EGFP was processed by the exchange with intact molecules from the cytoplasm (Fig. 4a). Fig. 4b shows the recovery curve averaged over 10 samples, and the nucleocytoplasmic transport k was estimated by fitting each normalised recovery with the single exponent (equation (4). From the recovery curve of fluorescence after photobleaching, the nucleocytoplasmic transport rate of EGFP (27 kDa) was measured to be $9.8 \pm 2.0 \times 10^{-3}$ s^{-1}. After EGFP photobleaching was completely recovered, we used the same cell to measure the transport rate under the 1 MHz LIPUS exposure with 400 kPa (Fig. 4b). When the LIPUS was applied during the whole recovery process after the photobleaching for 10 min, the nucleocytoplasmic transport rate of the EGFP increased by 20.9 % (Fig. 4c).

To exclude the possibility that the opening of nuclear pore complexes (NPCs) by LIPUS exposure may increase nuclear membrane permeability [54–56], we disrupted the linker of nucleus and cytoskeleton (LINC) complex which connects actin fibers to the nuclear lamina, and then examined whether the nucleocytoplasmic transport rate was affected by NPC structural changes. Nesprin [57], a family of proteins that are found primarily in the outer nuclear membrane, can mediate external force delivered from the cytoskeleton to the nucleus, and the force can modulate the mechanical process of NPCs' opening [56]. To block the LINC complex by nesprin, mCherry labelled dominant negative form of nesprin KASH domain (DN-KASH) was overexpressed in SaOS-2 cells (Supplementary Fig. 3). In comparison to the control group, the nucleocytoplasmic transport rate of DN-KASH overexpressed SaOS-2 cells was reduced to $6.8 \pm 3.2 \times 10^{-3}$ s^{-1} (mean ± standard deviation, Fig. 4c), which is consistent to the previous study [54]. Notably, the increase of nucleocytoplasmic transport rate by the LIPUS stimulation was maintained regardless of DN-KASH overexpression (Fig. 4c). Taken together, we can therefore conclude that the LIPUS-induced acceleration of passive nucleocytoplasmic transport results from acoustically increased diffusivity of EGFP, rather than the modulation of LINC complex-dependent deformation of the nucleus membrane.

3.4. *LIPUS stimulation amplifies ERK reaction kinetics*

In the present study, we also tested whether LIPUS can increase the diffusion of protein enzymes into the cytoplasm and can affect their kinase activity. For this purpose, we chose extracellular signal-regulated kinase (ERK), a central regulator kinase of a variety of cellular processes. ERK plays a role in mitogen-activated protein kinase (MAPK) signaling cascades and transmits extracellular signals to diverse intracellular targets [58,59]. To monitor the ERK-activation dynamics, a genetically encoded FRET biosensor, cytoplasmic EKAR whose conformational rearrangement by phosphorylation enhances the FRET signal, was used [32]. The FRET efficiency which was defined by the ratio of I_{DA}/I_{DD} (see

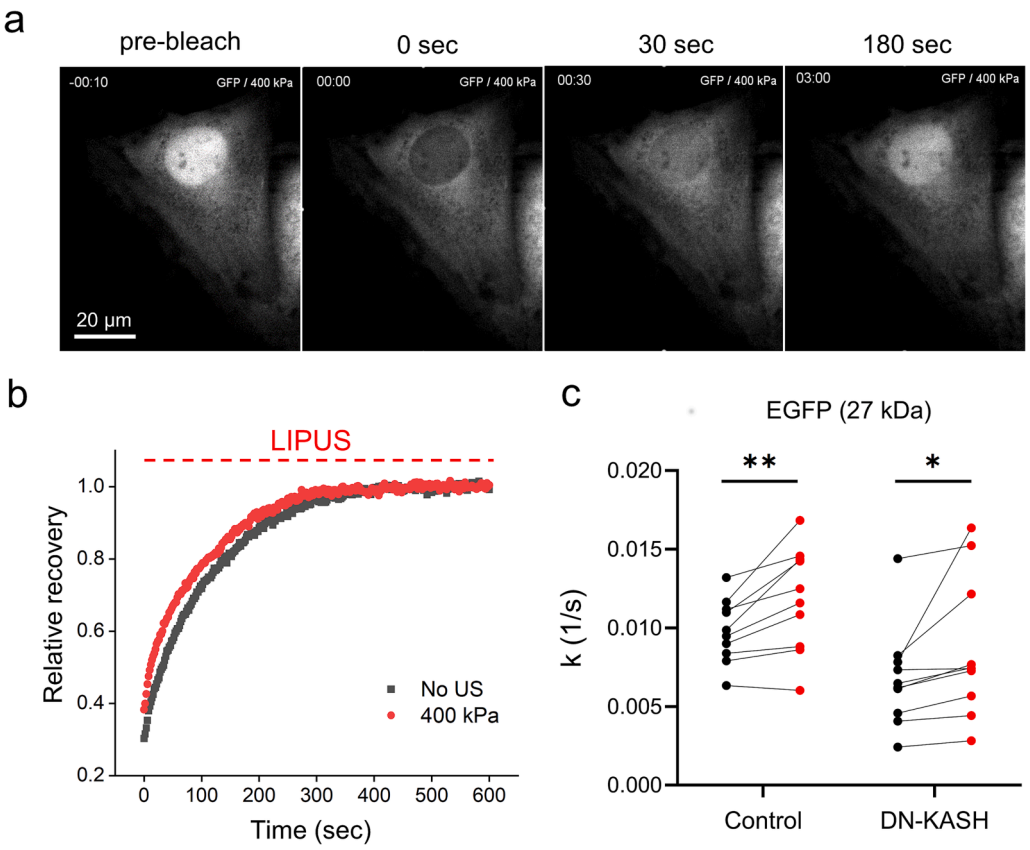

Fig. 4. FRAP analysis to measure the nucleocytoplasmic transport rate of EGFP. (a) Fluorescence images of EGFP labelled SaOS-2 cells before and after photobleaching (b) Time-dependent fluorescence intensity of SaOS-2 cells in the absence (black) or presence (red) of LIPUS exposure. (c) Nucleocytoplasmic transport rate *k* of EGFP in the absence (black) or presence (red) of LIPUS stimulation. In case of DN-KASH, SaOS-2 cells were co-transfected with EGFP and mCherry labelled DN-KASH, and the cells with mCherry fluorescence were selected for FRAP measurements. ($n = 9$ independent experiments each for the control and DN-KASH group, respectively, paired *t*-test). Values are expressed as mean ± SD of 9 samples. * $P < 0.05$ and ** $P < 0.01$. (For interpretation of the references to colour in this figure legend, the reader is referred to the web version of this article.)

Materials and Methods 2.10) was monitored before and after epidermal growth factor (EGF) treatment (Fig. 5a). Before the kinetic measurements, the diffusivity of the GFP-tagged ERK1(GFP-ERK1, 71 kDa) was initially measured by FRAP analysis. We observed that the diffusion coefficient of GFP-ERK1 increased by 27.3 % with the 1 MHz LIPUS exposure (400 kPa) (Fig. 5b), which was consistent with the previous measurements with similar molecular weight (shown in Fig. 2b). Next, to observe LIPUS dependent EKR activation dynamics, SaOS-2 cells were transfected with ERK FRET sensor, cytoplasmic EKAR (EGFP-mRFP) plasmid, which shows increased FRET by ERK phosphorylation. The signaling cascade was initiated by EGF treatment (50 μg/mL) followed by a 5 mins-long LIPUS exposure (1 MHz with 400 kPa).

Distinct temporal changes of ERK activation were observed in the corresponding FRET signal shown in Fig. 5c. The ERK phosphorylation induced by EGF increased by the LIPUS stimulation, and the level was maintained over 10 min after reaching the peak point (indicated by the red line in Fig. 5c), whereas we observed a gradual decline of the ERK in the absence of the LIPUS exposure (indicated by the black line in Fig. 5c). There seems no significant differences in the onset and the slope of EGF-induced FRET signal risings that occurred around 2 min between with or without the LIPUS exposure (between the red and black lines in Fig. 5c). Furthermore, when we solely applied the LIPUS to SaOS-2 cells without the EGF treatment, the ERK activity was rarely observed (indicated by the blue line in Fig. 5c). This can exclude the possibility that LIPUS directly activates the membrane receptors initiating ERK cascade. Our findings thus suggest that LIPUS can amplify the ERK activity by increasing its cytoplasmic diffusivity.

4. Discussion

In the present study, we (a) investigated how the diffusivity of intracellular macromolecules can be affected by LIPUS exposure and its possible effect on cellular processes, (b) and proposed an additional possible mechanism of LIPUS stimulation, which is shown in Fig. 6. It was clearly observed that LIPUS stimulation enhanced the diffusion coefficient of various macromolecules by ranging from 12.1 % to 33.5 %, depending on their molecular weight and acoustic pressure of LIPUS (Fig. 2c). Interestingly, there was a positive correlation between molecular weight and percentage increase of diffusivity upon LIPUS stimulation, and the trend was maintained regardless of the LIPUS driving frequency (Fig. 2c and Fig. 3d). The acoustically-increased diffusion of EGFP by LIPUS exposure led to a 21.4 % increase of its passive nucleocytoplasmic transport rate (Fig. 4). The increased diffusivity of ERK by LIPUS further amplified ERK activity which was initially triggered by EGF (Fig. 5). From these experimental results, it can be suggested that LIPUS can extensively modify cellular processes by increasing the diffusivities of various macromolecules within the intracellular region.

The LIPUS-increased diffusivity observed in the present study (Fig. 2b and 3c) is most likely to be due to the mechanical effects of LIPUS, since a significant temperature rise at the treatment site was not observed during the sonication. Acoustic cavitation, acoustic radiation force and acoustic streaming can be considered as major mechanical effects induced by ultrasound. During our experiments, however, no violent acoustic cavitation would likely occur; otherwise, significant cellular damage would have appeared. Since the range of molecular weights of the biomolecules used in this study was 4 to 500 kDa, the

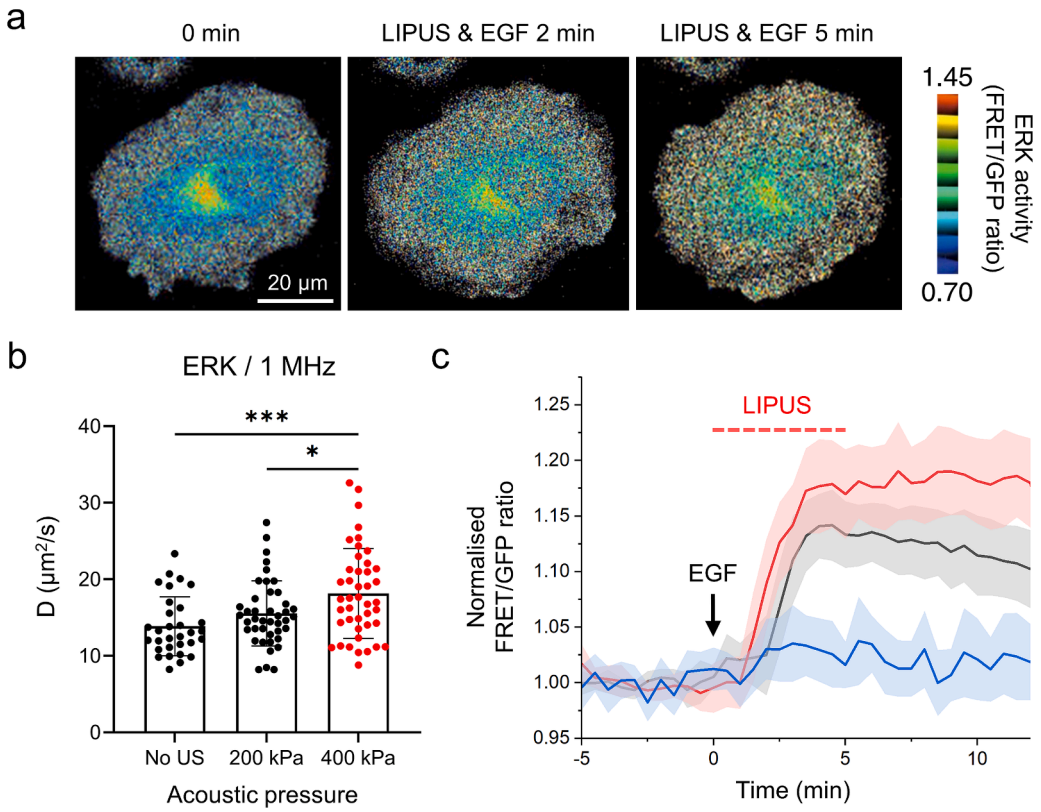

Fig. 5. (a) Representative FRET images EKAR biosensor (substrate of ERK) in SaOS-2 cells before and after 50 μM EGF and LIPUS stimulation (scale bar = 20 μm). (b) Increased diffusivity of ERK1 by LIPUS exposure. The statistically significant data is presented as red. (c) Time dependent normalized FRET/GFP ratio (see Material and Methods for details). Blue, black and red lines represent cells treated with LIPUS only (No EGF), EGF only (No LIPUS) and LIPUS + EGF, respectively. Solid lines represent the mean values and the shaded areas represent the SD. Values are expressed as mean ± SD of > 30 and > 19 samples, for FRAP and FRET experiments, respectively. * $P < 0.05$, ** $P < 0.01$, *** $P < 0.001$, **** $P < 0.0001$. (For interpretation of the references to colour in this figure legend, the reader is referred to the web version of this article.)

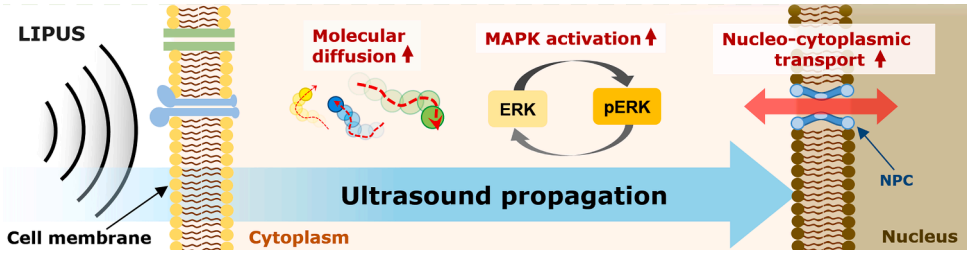

Fig. 6. Proposed mechanisms of LIPUS in the present study. LIPUS stimulation can increase diffusivity of cytoplasmic macromolecules, resulting in enhanced protein activity and nucleocytoplasmic transport rate.

largest one was assumed to be a sphere particle with a radius of 5 nm. The size of the particle (sub nanoscale) and the difference of acoustic impedance with the surrounding fluid were, however, too small to generate acoustic radiation force, inducing a directional motion of the particle through the wave-particle interaction [60,61]. In addition, although oscillatory diffusion is conceivable, the case of a weak solution at GUV (<1% w/v) hardly fulfils the basic assumption that the surrounding of probe particles is a poroelastic environment [62,63].

The physical basis for the increase in the molecular diffusivity during the LIPUS radiation is possibly derived from the mechanical stress that is transmitted across cell and vesicle lipid membrane. The viscous friction between the lipid membrane and the acoustic streaming of the surrounding medium can induce the motion and deformation of lipid membrane. In the cases of lipid vesicles, the mechanical stresses induced by unidirectional flow or ultrasound have been shown to transmit into the lumen area, producing internal streaming within the vesicles [64]. Ultrasound-induced acoustic radiation force can also deform and oscillate the cell membrane directly [15]. The radiation force induced by a 10 ms of 1 MHz burst continuous ultrasound with 185 kPa directly deflected the lipid membrane up to about 170 nm, and the mechanical response of the membrane was predicted to oscillate at a frequency far less than the incident ultrasound [15]. The slow response (kilo Hertz order) not only corresponds to the frequency range of action potentials induced by ultrasound but also proposes that the membrane dissipates mechanical energy partially into viscous force, which may assist the molecular diffusion process in the vicinity solution.

In addition, ultrasound waves may directly impact macromolecular dynamics. When ultrasound propagates through a complex solution, the media absorbs the part of acoustic energy by solute solvent interaction [65,66]. Each molecular content within the solution has a different translational relaxation time, suggesting that ultrasound causes relative motion between them (a mechanical momentum exchange). When

ultrasonic pulses impinge on microparticles dispersed in a liquid, ultrasonic scattering from the particles can be observed, albeit at a very low intensity [67]. It has been observed that the motions of 25-nm-sized silica particles were greatly accelerated by pulsed ultrasound [68]. Furthermore, ultrasound can enhance the cooperative local motions of the solvent protein molecules (including diffusive motion) while the macroscopic temperature of the system remains unchanged [69]. On the basis of these, the attenuation of ultrasonic scattering within nanoscale particle suspensions (i.e., colloidal suspensions) can be possibly correlated with the acceleration of molecular dynamics. Experimental and theoretical investigations on ultrasonic scattering in a suspension of nanoscale silica particles have shown that the attenuation of particles with diameters below 1 μm is generally proportional to ultrasonic frequency and particle size [70,71]. Baudoin et al. showed that the acoustic attenuation of suspension of silica particles with a 70 nm diameter (comparable particle size to macromolecules) was about five times greater than that of 35 nm [72]. The values were successfully compared with the simulation that accounted for the visco-inertial effects caused by velocity and thermal capacity differences between particles and the surrounding liquid. Therefore, scattering attenuation may be responsible for our results showing the positive correlation between molecular weight and the percentage increase of diffusivity upon LIPUS stimulation (Fig. 2c and 3d).

In the present study, no dependence of diffusivity changes on LIPUS frequency (varied from 0.5 to 3 MHz) was observed (Fig. 2c). This is most likely to be due to the relationship between attenuation of acoustic scattering and the size of biomolecules (nanoscale particles). The conventional multiple scattering theory often overestimates acoustic attenuation in suspensions as the particle size approaches the nanometer scale (less attenuation measured than prediction) [73]. Through the investigations on acoustic attenuation over a wide frequency range of 1–100 MHz, the attenuation in suspensions of nanoscale silica particles with 100 nm diameter, as opposed to macro-sized particles, was measured to be lower than the value predicted by the conventional model [71]. Correspondingly, the attenuation change of nanoscale particles as a function of frequency in the low frequency region (1–5 MHz) was significantly lower than that in the high frequency range [71]. The Stokes diameters of the macromolecules used in the present study were in the range of 2 to 15 nm, so the dependence under the LIPUS frequencies of 0.5 to 3 MHz used in the experiments may, therefore, be insignificant, which can possibly explain our experimental results shown in Fig. 2c and 3d.

Biological context of molecular diffusivity changes caused by other external stresses such as osmotic pressure [74], heat shock [75], and hypergravity [76] has been reported. Osmotic pressure directly modifies intracellular viscosity by regulating the water content, which causes changes in the diffusivity of various macromolecules within the cell. The polymerisation of microtubules (MT) is strongly dependent on the diffusion of tubulin molecules (100 kDa), and the diffusion and polymerisation rates in yeast protoplasts increased up to about 50 % by hypoosmotic shock with 0.2 M sorbitol [26]. In contrast, hyperosmotic compression slowed down various cellular dynamic processes, including protein diffusion, signal transduction and nuclear translocation [74]. These can possibly imply that there is a positive relationship between diffusivity changes of functional biomolecules and intracellular processes. In our experiments, it was clearly observed that the diffusivity increased by LIPUS exposure (Fig. 2), which in turn may lead to an increase in cellular dynamic processes (Figs. 4 and 5). Of course, additional studies focussing on each diffusion-dependent cellular process and their interplays are needed to further understand the impacts of LIPUS-induced diffusivity changes on cell function.

It has been reported that the passive nucleocytoplasmic transport rate can be physically modulated by applying mechanical force. For example, mechanical cues such as force application [55], substrate stiffness [77] and topography [78] could directly control the passive nucleus transport process. These statically or quasi-statically applied forces are delivered through the cytoskeleton to the nucleus membrane, resulting in the structural changes of NPC. Therefore, disruption of LINC by DN-KASH expression can abolish these mechanical effects [54,79]. On the other hand, our result implies that the increased transport rate by LIPUS originated from the increased molecular diffusivity rather than physically regulating LINC-dependent structural changes of NPC (Fig. 4c) [80]. Fick's first law of diffusion, which describes the mass flux of the permeates through the membrane, states that the flux is proportional to the permeates' self-diffusivity. The two comparable increases in EGFP's diffusivity in the cytoplasm (15.8 %, Fig. 2d) and nucleocytoplasmic transport rate (20.9 %, Fig. 3c) could mean that the flux of EGFP through the nuclear membrane is enhanced in line with its diffusivity. Meanwhile, various mechanical stimuli, including LIPUS, have been reported to enhance the nuclear translocation of YAP [81], a vital mechanosensitive transcriptional activator [82,83]. These results have mainly been explained by mechanically widened NPCs through LINC [54,84]. However, due to the relatively comparable size of YAP (~54 kDa) for passive transport, it is also possible that the increased diffusion process mediates enhanced nuclear translocation [56]. Further investigation is necessary to clarify the detailed mechanism of YAP nuclear entry under LIPUS exposure.

The enhanced phosphorylation of ERK substrate by LIPUS stimulation (Fig. 5) demonstrated that LIPUS stimulation can possibly regulate the kinase activity followed by the signal transduction process. A numerical study reported that ultrasound has the potential to accelerate protein–ligand binding kinetics through a solvent-mediated mechanism without denaturalising the protein structure [69]. There also are studies that the kinase's signaling cascade can be regulated by the diffusivity of molecules involved [85–87]. Still, assessing the effect of increased diffusion of macromolecules, including ERK by LIPUS, on the whole MAPK/ERK signal transduction is challenging. This is because LIPUS may impact the different dynamics of the multiple components of the pathway; not only ERK but also complex crosstalk with other pathways also exists. Radiating LIPUS on a cell-free kinase assay could effectively help understand whether and how kinase kinetics are directly altered by ultrasound waves [88]. On top of that, eukaryotic cells overcome a large spatial gradient [89–91] of kinase localization not only by passive diffusion but also by many other dynamical strategies, including phase separation [92], molecular crowding [93] and endocytic trafficking [94]. Further investigation into the LIPUS effects on the general kinase activity in the signaling pathway would flourish our understanding of acoustically modulated signaling transduction.

5. Conclusion

In this study, for the first time in the fields of LIPUS, we reported the increased diffusivity of intracellular macromolecules by LIPUS stimulation. During the sonication, the diffusivity enhancement of FITC-dextran, ranging from 4 to 500 kDa, increased with acoustic pressure, and the percentage of increase was proportional to the molecular weight of the probes. The comparison with the diffusion of macromolecules within a GUV (a cell-mimicking model) showed the same trend of diffusivity enhancement with living cells, which indicates that this phenomenon is a physical reaction. LIPUS acoustically increased the rate of passive nucleocytoplasmic transport of EGFP and intensified the phosphorylation of ERK together with its diffusivity. This implies that cell biological effects of LIPUS can be initiated by physical property changes in the intracellular area. Our findings open up new perspectives in mechanobiology in that mechanical stress can accelerate pre-existing cellular processes, not only triggering specific signal pathways. Furthermore, taken together, our results provide the possibility of developing new technologies that can noninvasively control nanoscale dynamics inside cells.

CRediT authorship contribution statement

Hyojun Kim: Conceptualization, Formal analysis, Methodology, Data curation, Investigation, Writing – original draft. **Yeonho Choi:** Supervision. **So Yeon Kim:** Conceptualization, Formal analysis, Funding acquisition, Investigation, Supervision, Writing – review & editing. **Ki Joo Pahk:** Conceptualization, Formal analysis, Funding acquisition, Investigation, Supervision, Writing – review & editing.

Declaration of Competing Interest

The authors declare that they have no known competing financial interests or personal relationships that could have appeared to influence the work reported in this paper.

Data availability

Data will be made available on request.

Acknowledgements

This work was supported by the National Research Foundation of Korea (NRF) grant funded by the Korea government (MSIT) (No. NRF-2021R1C1C1008240 and 2021R1A2C2008897) and KIST grant (2E32332). This work was also supported by the Korea Medical Device Development Fund grant funded by the Korea government (the Ministry of Science and ICT, the Ministry of Trade, Industry and Energy, the Ministry of Health & Welfare, the Ministry of Food and Drug Safety) (Project Number: RS-2022-00141091).

Appendix A. Supplementary data

Supplementary data to this article can be found online at https://doi.org/10.1016/j.ultsonch.2023.106644.

References

[1] G. Ter Haar, Therapeutic applications of ultrasound, Prog. Biophys. Mol. Biol. 93 (2007) 111–129.
[2] K.G. Baker, V.J. Robertson, F.A. Duck, A review of therapeutic ultrasound: biophysical effects, Phys. Ther. 81 (2001) 1351–1358.
[3] A. Harrison, S. Lin, N. Pounder, Y. Mikuni-Takagaki, Mode & mechanism of low intensity pulsed ultrasound (LIPUS) in fracture repair, Ultrasonics 70 (2016) 45–52.
[4] B. Vafaeian, M. El-Rich, T. El-Bialy, S. Adeeb, The finite element method for micro-scale modeling of ultrasound propagation in cancellous bone, Ultrasonics 54 (2014) 1663–1676.
[5] A. Binder, G. Hodge, A. Greenwood, B. Hazleman, D.P. Thomas, Is therapeutic ultrasound effective in treating soft tissue lesions? Br. Med. J. (Clin. Res. Ed) 290 (1985) 512–514.
[6] A. Khanna, R.T. Nelmes, N. Gougoulias, N. Maffulli, J. Gray, The effects of LIPUS on soft-tissue healing: a review of literature, Br. Med. Bull. 89 (2009) 169–182.
[7] N.Z. Mostafa, H. Uludağ, D.N. Dederich, M.R. Doschak, T.H. El-Bialy, Anabolic effects of low-intensity pulsed ultrasound on human gingival fibroblasts, Arch. Oral Biol. 54 (2009) 743–748.
[8] C.S. Enwemeka, O. Rodriguez, S. Mendosa, The biomechanical effects of low-intensity ultrasound on healing tendons, Ultrasound Med. Biol. 16 (1990) 801–807.
[9] T. Nakamura, S. Fujihara, K. Yamamoto-Nagata, T. Katsura, T. Inubushi, E. Tanaka, Low-intensity pulsed ultrasound reduces the inflammatory activity of synovitis, Ann. Biomed. Eng. 39 (2011) 2964–2971.
[10] W.J. Tyler, Y. Tufail, M. Finsterwald, M.L. Tauchmann, E.J. Olson, C. Majestic, Remote excitation of neuronal circuits using low-intensity, low-frequency ultrasound, PLoS One 3 (2008) e3511.
[11] T. El-Bialy, A. Alhadlaq, B. Wong, C. Kucharski, Ultrasound effect on neural differentiation of gingival stem/progenitor cells, Ann. Biomed. Eng. 42 (2014) 1406–1412.
[12] X. Jiang, O. Savchenko, Y. Li, S. Qi, T. Yang, W. Zhang, J. Chen, A review of low-intensity pulsed ultrasound for therapeutic applications, IEEE Trans. Biomed. Eng. 66 (2018) 2704–2718.
[13] T. Watson, Ultrasound in contemporary physiotherapy practice, Ultrasonics 48 (2008) 321–329.
[14] Y.-C. Chu, J. Lim, A. Chien, C.-C. Chen, J.-L. Wang, Activation of Mechanosensitive Ion Channels by Ultrasound, Ultrasound Med. Biol. (2022).
[15] M.L. Prieto, Ö. Oralkan, B.T. Khuri-Yakub, M.C. Maduke, Dynamic response of model lipid membranes to ultrasonic radiation force, PLoS One 8 (2013) e77115.
[16] A. Vasan, J. Orosco, U. Magaram, M. Duque, C. Weiss, Y. Tufail, S.H. Chalasani, J. Friend, Ultrasound mediated cellular deflection results in cellular depolarization, Adv. Sci. 9 (2022) 2101950.
[17] S. Yoo, D.R. Mittelstein, R.C. Hurt, J. Lacroix, M.G. Shapiro, Focused ultrasound excites cortical neurons via mechanosensitive calcium accumulation and ion channel amplification, Nat. Commun. 13 (2022) 1–13.
[18] R.J. Ellis, Macromolecular crowding: obvious but underappreciated, Trends Biochem. Sci. 26 (2001) 597–604.
[19] J.A. Dix, A. Verkman, Crowding effects on diffusion in solutions and cells, Annu. Rev. Biophys. 37 (2008) 247–263.
[20] Q. Feng, B. Kornmann, Mechanical forces on cellular organelles, J. Cell Sci. 131 (2018) jcs218479.
[21] S.C.J. Helle, Q. Feng, M.J. Aebersold, L. Hirt, R.R. Grüter, A. Vahid, A. Sirianni, S. Mostowy, J.G. Snedeker, A. Šarić, Mechanical force induces mitochondrial fission, Elife 6 (2017) e30292.
[22] B. Alric, C. Formosa-Dague, E. Dague, L.J. Holt, M. Delarue, Macromolecular crowding limits growth under pressure, Nat. Phys. 18 (2022) 411–416.
[23] M. Eigen, Diffusion control in biochemical reactions, in: Quantum Statistical Mechanics in the Natural Sciences, Springer, 1974, pp. 37–61.
[24] S. Soh, M. Byrska, K. Kandere-Grzybowska, B.A. Grzybowski, Reaction-diffusion systems in intracellular molecular transport and control, Angew. Chem. Int. Ed. 49 (2010) 4170–4198.
[25] O. Keminer, R. Peters, Permeability of single nuclear pores, Biophys. J. 77 (1999) 217–228.
[26] A.T. Molines, J. Lemière, M. Gazzola, I.E. Steinmark, C.H. Edrington, C.-T. Hsu, P. Real-Calderon, K. Suhling, G. Goshima, L.J. Holt, M. Thery, G.J. Brouhard, F. Chang, Physical properties of the cytoplasm modulate the rates of microtubule polymerization and depolymerization, Dev. Cell 57 (2022) 466–479, e466.
[27] D. Drenckhahn, T.D. Pollard, Elongation of actin filaments is a diffusion-limited reaction at the barbed end and is accelerated by inert macromolecules, J. Biol. Chem. 261 (1986) 12754–12758.
[28] M.C. Munder, D. Midtvedt, T. Franzmann, E. Nuske, O. Otto, M. Herbig, E. Ulbricht, P. Müller, A. Taubenberger, S. Maharana, A pH-Driven Transition of the Cytoplasm from a Fluid-to a Solid-like State Promotes Entry into Dormancy, Elife 5 (2016) e09347.
[29] J.D. Finan, H.A. Leddy, F. Guilak, Osmotic stress alters chromatin condensation and nucleocytoplasmic transport, Biochem. Biophys. Res. Commun. 408 (2011) 230–235.
[30] O.P. Hamill, D.W. Mcbride, The pharmacology of mechanogated membrane ion channels, Pharmacol. Rev. 48 (1996) 231–252.
[31] Y. Yung, Z. Yao, D.M. Aebersold, T. Hanoch, R. Seger, Altered regulation of ERK1b by MEK1 and PTP-SL and modified Elk1 phosphorylation by ERK1b are caused by abrogation of the regulatory C-terminal sequence of ERKs, J. Biol. Chem. 276 (2001) 35280–35289.
[32] C.D. Harvey, A.G. Ehrhardt, C. Cellurale, H. Zhong, R. Yasuda, R.J. Davis, K. Svoboda, A genetically encoded fluorescent sensor of ERK activity, Proc. Natl. Acad. Sci. 105 (2008) 19264–19269.
[33] C.R. Mayer, P.T. Arsenovic, K. Bathula, K.B. Denis, D.E. Conway, Characterization of 3D printed stretching devices for imaging force transmission in live-cells, Cell. Mol. Bioeng. 12 (2019) 289–300.
[34] P.L. McNEIL, E. Warder, Glass beads load macromolecules into living cells, J. Cell Sci. 88 (1987) 669–678.
[35] D. Arbelaez-Camargo, M. Roig-Carreras, E. García-Montoya, P. Pérez-Lozano, M. Miñarro-Carmona, J.R. Ticó-Grau, J.M. Suñé-Negre, Osmolality predictive models of different polymers as tools in parenteral and ophthalmic formulation development, Int. J. Pharm. 543 (2018) 190–200.
[36] M. Kang, C.A. Day, K. Drake, A.K. Kenworthy, E. DiBenedetto, A generalization of theory for two-dimensional fluorescence recovery after photobleaching applicable to confocal laser scanning microscopes, Biophys. J. 97 (2009) 1501–1511.
[37] D. Axelrod, D. Koppel, J. Schlessinger, E. Elson, W.W. Webb, Mobility measurement by analysis of fluorescence photobleaching recovery kinetics, Biophys. J. 16 (1976) 1055–1069.
[38] M. Kang, C.A. Day, A.K. Kenworthy, E. DiBenedetto, Simplified equation to extract diffusion coefficients from confocal FRAP data, Traffic 13 (2012) 1589–1600.
[39] V. Pereno, D. Carugo, L. Bau, E. Sezgin, J. Bernardino de la Serna, C. Eggeling, E. Stride, Electroformation of giant unilamellar vesicles on stainless steel electrodes, ACS Omega 2 (2017) 994–1002.
[40] R. Bizzarri, F. Cardarelli, M. Serresi, F. Beltram, Fluorescence recovery after photobleaching reveals the biochemistry of nucleocytoplasmic exchange, Anal. Bioanal. Chem. 403 (2012) 2339–2351.
[41] G. Ferri, B. Storti, R. Bizzarri, Nucleocytoplasmic transport in cells with progerin-induced defective nuclear lamina, Biophys. Chem. 229 (2017) 77–83.
[42] Q. Qiu, M. Yang, B. Tsang, A. Gruslin, EGF-induced trophoblast secretion of MMP-9 and TIMP-1 involves activation of both PI3K and MAPK signalling pathways, Reproduction 128 (2004) 355–363.
[43] B. Schoeberl, C. Eichler-Jonsson, E.D. Gilles, G. Müller, Computational modeling of the dynamics of the MAP kinase cascade activated by surface and internalized EGF receptors, Nat. Biotechnol. 20 (2002) 370–375.
[44] Y. Blum, R.D. Fritz, H. Ryu, O. Pertz, Measuring ERK activity dynamics in single living cells using FRET biosensors, ERK Signaling, Springer, in, 2017, pp. 203–221.
[45] S. Popov, M. Poo, Diffusional transport of macromolecules in developing nerve processes, J. Neurosci. 12 (1992) 77–85.
[46] W.Y. Huang, X. Cheng, J.E. Ferrell, Cytoplasmic organization promotes protein diffusion in Xenopus extracts, Nat. Commun. 13 (2022) 1–10.
[47] O. Seksek, J. Biwersi, A. Verkman, Translational diffusion of macromolecule-sized solutes in cytoplasm and nucleus, J. Cell Biol. 138 (1997) 131–142.

[48] Z. Qiu, J. Guo, S. Kala, J. Zhu, Q. Xian, W. Qiu, G. Li, T. Zhu, L. Meng, R. Zhang, The mechanosensitive ion channel Piezo1 significantly mediates in vitro ultrasonic stimulation of neurons, Iscience 21 (2019) 448–457.
[49] S. Jeong, H.T. Nguyen, C.H. Kim, M.N. Ly, K. Shin, Toward artificial cells: novel advances in energy conversion and cellular motility, Adv. Funct. Mater. 30 (2020) 1907182.
[50] S.F. Fenz, K. Sengupta, Giant vesicles as cell models, Integr. Biol. 4 (2012) 982–995.
[51] A.S. Verkman, Solute and macromolecule diffusion in cellular aqueous compartments, Trends Biochem. Sci 27 (2002) 27–33.
[52] E.A. Nigg, Nucleocytoplasmic transport: signals, mechanisms and regulation, Nature 386 (1997) 779–787.
[53] T. Nguyen, N. Pappireddi, M. Wühr, Proteomics of nucleocytoplasmic partitioning, Curr. Opin. Chem. Biol. 48 (2019) 55–63.
[54] I. Andreu, I. Granero-Moya, N.R. Chahare, K. Clein, M. Molina-Jordán, A.E. Beedle, A. Elosegui-Artola, J.F. Abenza, L. Rossetti, X. Trepat, Mechanical force application to the nucleus regulates nucleocytoplasmic transport, Nat. Cell Biol. (2022) 1–10.
[55] I. Andreu, I. Granero-Moya, S. Garcia-Manyes, P. Roca-Cusachs, Understanding the role of mechanics in nucleocytoplasmic transport, APL Bioeng. 6 (2022), 020901.
[56] A. Elosegui-Artola, I. Andreu, A.E. Beedle, A. Lezamiz, M. Uroz, A.J. Kosmalska, R. Oria, J.Z. Kechagia, P. Rico-Lastres, A.-L. Le Roux, Force triggers YAP nuclear entry by regulating transport across nuclear pores, Cell 171 (2017) 1397–1410, e1314.
[57] Q. Zhang, J.N. Skepper, F. Yang, J.D. Davies, L. Hegyi, R.G. Roberts, P. L. Weissberg, J.A. Ellis, C.M. Shanahan, Nesprins: a novel family of spectrin-repeat-containing proteins that localize to the nuclear membrane in multiple tissues, J. Cell Sci. 114 (2001) 4485–4498.
[58] H. Rubinfeld, R. Seger, The ERK cascade, Mol. Biotechnol. 31 (2005) 151–174.
[59] H. Lavoie, J. Gagnon, M. Therrien, ERK signalling: a master regulator of cell behaviour, life and fate, Nat. Rev. Mol. Cell Biol. 21 (2020) 607–632.
[60] C. Reyes, L. Fu, P.P. Suthanthiraraj, C.E. Owens, C.W. Shields IV, G.P. López, P. Charbonneau, B.J. Wiley, The Limits of Primary Radiation Forces in Bulk Acoustic Standing Waves for Concentrating Nanoparticles, Part. Part. Syst. Char. 35 (2018) 1700470.
[61] H. Bruus, Acoustofluidics 7: The acoustic radiation force on small particles, Lab Chip 12 (2012) 1014–1021.
[62] A. Karki, J.S. Marshall, J. Wu, Effect of ultrasound amplitude and frequency on nanoparticle diffusion in an agarose hydrogel, J. Acoust. Soc. Am. 152 (2022) 640–650.
[63] J.S. Marshall, C. Arnold, K. Curran, T. Chivers, Statistics of particle diffusion subject to oscillatory flow in a porous bed, Chem. Eng. Sci. 231 (2021), 116239.
[64] V. Pereno, J. Lei, D. Carugo, E. Stride, Microstreaming inside model cells induced by ultrasound and microbubbles, Langmuir 36 (2020) 6388–6398.
[65] T. Liu, S. Wang, M. Zhu, Predicting acoustic relaxation absorption in gas mixtures for extraction of composition relaxation contributions, Proc. Royal Soc. A: Math. Phys. Eng. Sci. 473 (2017) 20170496.
[66] S. Azhagiri, S. Jayakumar, R. Padmanaban, S. Gunasekaran, S. Srinivasan, Acoustic and thermodynamic properties of binary liquid mixtures of benzaldehyde in hexane and cyclohexane, J. Solution Chem. 38 (2009) 441–448.
[67] J. Page, M. Cowan, D. Weitz, Diffusing acoustic wave spectroscopy of fluidized suspensions, Phys. B Condens. Matter 279 (2000) 130–133.
[68] K. Kitao, T. Norisuye, Nanoparticle sizing by focused-beam dynamic ultrasound scattering method, Ultrasonics 126 (2022), 106807.
[69] M. Araki, S. Matsumoto, G.-J. Bekker, Y. Isaka, Y. Sagae, N. Kamiya, Y. Okuno, Exploring ligand binding pathways on proteins using hypersound-accelerated molecular dynamics, Nat. Commun. 12 (2021) 2793.
[70] D.M. Forrester, J. Huang, V.J. Pinfield, F. Luppé, Experimental verification of nanofluid shear-wave reconversion in ultrasonic fields, Nanoscale 8 (2016) 5497–5506.
[71] D.M. Forrester, J. Huang, V.J. Pinfield, Characterisation of colloidal dispersions using ultrasound spectroscopy and multiple-scattering theory inclusive of shear-wave effects, Chem. Eng. Res. Des. 114 (2016) 69–78.
[72] M. Baudoin, J.-L. Thomas, F. Coulouvrat, C. Chanéac, Scattering of ultrasonic shock waves in suspensions of silica nanoparticles, J. Acoust. Soc. Am. 129 (2011) 1209–1220.
[73] K. Kobayashi, T. Norisuye, K. Sugita, H. Nakanishi, Q. Tran-Cong-Miyata, Dynamics of nanometer-and submicrometer-sized particles in suspension probed by dynamic ultrasound scattering techniques, J. Appl. Phys. 122 (2017).
[74] A. Miermont, F. Waharte, S. Hu, M.N. McClean, S. Bottani, S. Léon, P. Hersen, Severe osmotic compression triggers a slowdown of intracellular signaling, which can be explained by molecular crowding, Proc. Natl. Acad. Sci., 110 (2013) 5725-5730.
[75] L.B. Persson, V.S. Ambati, O. Brandman, Cellular control of viscosity counters changes in temperature and energy availability, Cell 183 (2020) 1572–1585, e1516.
[76] E.M. Woodcock, P. Girvan, J. Eckert, I. Lopez-Duarte, M. Kubánková, J.J. van Loon, N.J. Brooks, M.K. Kuimova, Measuring intracellular viscosity in conditions of hypergravity, Biophys. J . 116 (2019) 1984–1993.
[77] A. Elosegui-Artola, R. Oria, Y. Chen, A. Kosmalska, C. Pérez-González, N. Castro, C. Zhu, X. Trepat, P. Roca-Cusachs, Mechanical regulation of a molecular clutch defines force transmission and transduction in response to matrix rigidity, Nat. Cell Biol. 18 (2016) 540–548.
[78] E. Jacchetti, R. Nasehi, L. Boeri, V. Parodi, A. Negro, D. Albani, R. Osellame, G. Cerullo, J.F.R. Matas, M.T. Raimondi, The nuclear import of the transcription factor MyoD is reduced in mesenchymal stem cells grown in a 3D micro-engineered niche, Sci. Rep. 11 (2021) 1–19.
[79] J. Aureille, N. Belaadi, C. Guilluy, Mechanotransduction via the nuclear envelope: a distant reflection of the cell surface, Curr. Opin. Cell Biol. 44 (2017) 59–67.
[80] C. Colton, K. Smith, E. Merrill, P. Farrell, Permeability studies with cellulosic membranes, J. Biomed. Mater. Res. 5 (1971) 459–488.
[81] S. Dupont, L. Morsut, M. Aragona, E. Enzo, S. Giulitti, M. Cordenonsi, F. Zanconato, J. Le Digabel, M. Forcato, S. Bicciato, Role of YAP/TAZ in mechanotransduction, Nature 474 (2011) 179–183.
[82] X.-M. Xu, T.-M. Xu, Y.-B. Wei, X.-X. Gao, J.-C. Sun, Y. Wang, Q.-J. Kong, J.-G. Shi, Low-intensity pulsed ultrasound treatment accelerates angiogenesis by activating YAP/TAZ in human umbilical vein endothelial cells, Ultrasound Med. Biol. 44 (2018) 2655–2661.
[83] R. Puts, P. Rikeit, K. Ruschke, P. Knaus, S. Schreivogel, K. Raum, Functional regulation of YAP mechanosensitive transcriptional coactivator by Focused Low-Intensity Pulsed Ultrasound (FLIPUS) enhances proliferation of murine mesenchymal precursors, PLoS One 13 (2018) e0206041.
[84] T.J. Kirby, J. Lammerding, Emerging views of the nucleus as a cellular mechanosensor, Nat. Cell Biol. 20 (2018) 373–381.
[85] M. Sabouri-Ghomi, A. Ciliberto, S. Kar, B. Novak, J.J. Tyson, Antagonism and bistability in protein interaction networks, J. Theor. Biol. 250 (2008) 209–218.
[86] L. Qiao, R.B. Nachbar, I.G. Kevrekidis, S.Y. Shvartsman, Bistability and oscillations in the Huang-Ferrell model of MAPK signaling, PLoS Comput. Biol. 3 (2007) e184.
[87] Q. Zhao, M. Yi, Y. Liu, Spatial distribution and dose–response relationship for different operation modes in a reaction–diffusion model of the MAPK cascade, Phys. Biol. 8 (2011), 055004.
[88] M. Blazek, T.S. Santisteban, R. Zengerle, M. Meier, Analysis of fast protein phosphorylation kinetics in single cells on a microfluidic chip, Lab Chip 15 (2015) 726–734.
[89] B.N. Kholodenko, G.C. Brown, J.B. Hoek, Diffusion control of protein phosphorylation in signal transduction pathways, Biochem. J 350 (2000) 901–907.
[90] B.N. Kholodenko, Spatially distributed cell signalling, FEBS Lett. 583 (2009) 4006–4012.
[91] H.M. York, J. Coyle, S. Arumugam, To be more precise: the role of intracellular trafficking in development and pattern formation, Biochem. Soc. Trans. 48 (2020) 2051–2066.
[92] C.F. Lee, C.P. Brangwynne, J. Gharakhani, A.A. Hyman, F. Jülicher, Spatial organization of the cell cytoplasm by position-dependent phase separation, Phys. Rev. Lett. 111 (2013), 088101.
[93] J. Spitzer, B. Poolman, The role of biomacromolecular crowding, ionic strength, and physicochemical gradients in the complexities of life's emergence, Microbiol. Mol. Biol. Rev. 73 (2009) 371–388.
[94] A. Einstein, Uber die von der Molekularkinetischen Theorie der Warme Geforderte Bewegung von in Ruhenden Flussigkeiten Suspendierten Teilchen (English translation: On the Movement of Small Particles Suspended in a Stationary Liquid Demanded by the Molecular-Kinetic Theory of Heat). Investigations on the Theory of the Brownian Movement, Dover, New York, 1905.